OPEN ACCESS

University of BRISTOL

Jeffrey, M. R., Hall, C. L., & Catsis, S. (2023). *The hidden sensitivity of non-smooth dynamics*. SSRN. https://doi.org/10.2139/ssrn.4626480

Early version, also known as pre-print

License (if available):
Unspecified

Link to published version (if available):
10.2139/ssrn.4626480

Link to publication record in Explore Bristol Research
PDF-document

This is a pre-print version of the article (version of record). It first appeared online via SSRN at http://dx.doi.org/10.2139/ssrn.4626480. Please refer to any applicable terms of use of the publisher.

University of Bristol - Explore Bristol Research
General rights

This document is made available in accordance with publisher policies. Please cite only the published version using the reference above. Full terms of use are available:
http://www.bristol.ac.uk/red/research-policy/pure/user-guides/ebr-terms/

The hidden sensitivity of non-smooth dynamics

Salvador Catsis, Cameron L. Hall, Mike R. Jeffrey *

January 26, 2024

Abstract

Switches in dynamical systems are known to exhibit wildly different behaviours depending on how they are modelled, for instance whether they occur as smooth transitions or abrupt jumps, and whether they involve delays or discrete perturbations. These differences arise because switches are sensitive to perturbation, but there is limited knowledge about where this sensitivity comes from. Here we take a switch in a simple one-dimensional system, then discretise time and introduce a small delay. The resulting system is described by a piecewise-linear map with incredibly complex dynamics, and is sensitive to parameter changes even if the time-steps and delays are made infinitesimally small. We show that this sensitivity reveals itself in the more versatile numerical tool of the *transition count*, which captures the likelihood of switching occurring at any instant in a simulation. We use this to show that sensitivity to parameters persists in a system with two switches, where it then has large-scale dynamical effects. The use of transition counts in this way may prove a versatile tool for studying more complex switching processes in general.

*Department of Engineering Mathematics, University of Bristol, Ada Lovelace Building, Bristol BS8 1TW, UK, email: mike.jeffrey@bristol.ac.uk

Contents

1 Introduction **3**

2 A single switch in discrete time with delay **6**

3 The many topologies of the 1D map **7**
3.1 The case $\phi > 1$ . . . 9
3.2 The case $\phi < 1$ . . . 11
3.3 Dynamics of the 1D map . . . 11

4 Transition counts **14**
4.1 Transition counts for one switch . . . 15
4.2 Transition counts for two switches . . . 18

5 Fine-scale process and large-scale sliding **20**
5.1 Sliding with one switch . . . 21
5.2 Sliding with two switches . . . 23

6 Other switching processes **26**
6.1 Isolated processes . . . 27
6.2 Smoothing and hysteresis . . . 28
6.3 Discretization and hysteresis . . . 28
6.4 Discretization and smoothing . . . 29

7 Closing remarks **30**
7.1 On sensitivity of nonsmooth dynamics . . . 30
7.2 On transition counts versus time spent in modes . . . 31
7.3 On types of switching . . . 31

A The sampling problem **33**

1 Introduction

Many real-world dynamical systems exhibit sharp transitions between different modes of behaviour. These transitions are often idealised as instantaneous switches between well-understood dynamical laws.

The most widely used method to simulate or analyse such switches is to approximate them using either discontinuous step functions, or smooth sigmoid functions, common choices being a hyperbolic tangent in neural networks [22, 33], a Hill function in biology [15, 12], or a C^∞ function in Sotomayor-Teixeira regularisation [28]. Under strong enough restrictions, it can be proven that sigmoid approximations give the same behaviour as step functions in an appropriate limit, and the results are consistent with so-called nonsmooth or 'Filippov' dynamics [28]. However, there are many situations where such approximations diverge from each other significantly, resulting in conflicting expectations of the dynamics, due to 'hidden dynamics' associated with the switch [14, 26, 17].

In these situations, it becomes necessary to consider more precisely the non-ideal processes that might be involved in switching. These might involve time delays or hysteresis in activating a switch, the effect of digital sampling, the effect of sensors, or system noise. No matter how small, such effects can entirely alter how a system will behave through a switch. As described in [17, 18], a discontinuous switch constitutes a singular limit, and any attempts to model the switch in more detail constitute singular perturbations that can result in widely conflicting behaviours.

Here we take a specific scenario where this singular limit can be explored in detail, showing why small changes in parameters can result in very different behaviour. Starting from a one-dimensional system with a discontinuous switch, we perturb the model by discretising the system, and applying a time delay to the activation of the switch. Both of these (the time-step and delay) can be made arbitrarily small. One such system can be found in [7], which studies genetic regulation in discrete time with delay.

Take a single variable that evolves according to $\dot{x} = a > 0$ for $x < 0$, and $\dot{x} = -b < 0$ for $x > 0$, ideally represented as

$$\dot{x} = a - (a + b)H(x) \,, \tag{1}$$

where H is the Heaviside step function. We will show that if x evolves in small time-steps $\delta t = \varepsilon$ and experiences a small delay of $\Delta t = \varepsilon\tau$ (note we will use δt and Δt to denote a time-step and a time-delay, respectively), for some small $\varepsilon > 0$ and any $\tau \in \mathbb{N}$, then it evolves according to the map

$$x \mapsto x + \varepsilon(aj - bk) \tag{2a}$$

where k and j are integers, given in a scaled coordinate $u = x/a\varepsilon$ and parameter $\phi = b/a$ by

$$k = \left\lceil \frac{u + \tau(1+\phi)}{\phi} \right\rceil , \qquad j = \lceil k\phi - u \rceil \ , \tag{2b}$$

where $\lceil z \rceil$ denotes the smallest integer such that $z \leq \lceil z \rceil$.

This seemingly simple result disguises an incredibly complex dynamical system. Despite involving just a piecewise-constant time-stepping algorithm, the map (2) is highly intricate, irrespective of how small the time-steps and delay are. The topology of the map changes with the values of τ and ϕ, and within any given topology the dynamics itself is highly complex. Maps of the form (2) are also known as *interval translations* [23, 5], a special case of piecewise linear maps [3].

After deriving this map and its parameter dependence, we show how this leads to variability in the *transition counts* of switching between system modes. We then show that, while such variability is constrained to a small neighbourhood around a single switch, it can have large-scale effects if there are two or more switches.

More precisely, we will show that if a system switches between two modes of evolution $(\dot{x}, \dot{y}) = (a, A)$ for $x > 0$, and $(\dot{x}, \dot{y}) = (-b, B)$ for $x > 0$, for $x \in \mathbb{R}$, $y \in \mathbb{R}^n$ and any $n \geq 1$, its dynamics over a sufficiently long time interval T takes the form

$$\begin{aligned} \dot{x} &= \mathcal{O}(\varepsilon) \ , \\ \dot{y} &= A + \{B - A\} \tfrac{1}{1+\phi} + \mathcal{O}\left(\frac{1}{T}\right) \ , \end{aligned} \tag{3}$$

hence it is well-defined for large T (where the process of switching between $x > 0$ and $x < 0$ takes place within a small region $|x| < \varepsilon \ll 1$). The expression (3) corresponds to Filippov's *sliding motion* or Utkin's *equivalent control* [10, 30, 17], to order ε.

In a system with two such switches, however, the dynamics along the thresholds is not so well-defined. Take two control variables, x_1 and x_2, both switching across $x_1 = 0$ and $x_2 = 0$, with the objective to reach $(x_1, x_2) = (0, 0)$ via a simple extension of (1) with parameters $\phi_1, \phi_2, \phi_3 > 0$, for example $\dot{x}_1 = 1 - (1 + \phi_1)H(x_1) - \phi_3 H(x_1)H(x_2)$ and $\dot{x}_2 = 1 - (1 + \phi_2)H(x_2) - \phi_3 H(x_1)H(x_2)$. In place of (3) we will show that the resulting

motion is given by

$$\begin{aligned} \dot{x}_1 &= \mathcal{O}(\varepsilon) \ , \\ \dot{x}_2 &= \mathcal{O}(\varepsilon) \ , \\ \dot{y} &= C_0 + C_1 \tfrac{1}{1+\phi_1} + C_2 \tfrac{1}{1+\phi_2} + C_3\mu + \mathcal{O}\left(\frac{1}{T}\right) \ , \qquad (4) \\ \text{where} \qquad \mu &\in [0,1] \ , \end{aligned}$$

where the C_i are just vector fields generalising the A and $B-A$ of (3). The salient point here at that, while the error term $\mathcal{O}(1/T)$ is small for large enough T, there is now also a multiplier μ that is indeterminable, and can lie anywhere in $[0,1]$. The value of μ is determined by the dynamics of a map that, unlike (2), is not known explicitly, but can similarly be expected to vary with parameters in a manner that does not disappear in the limit $\varepsilon \to 0$, and we verify this numerically. That is to say, μ may vary over $\mu \in [0,1]$, so the y dynamics may vary over a range satisfying

$$\dot{y} - \left(C_0 + C_1 \tfrac{1}{1+\phi_1} + C_2 \tfrac{1}{1+\phi_2}\right) \in [0,1]\, C_3 \ ,$$

where C_3 can be of any size and direction, no matter how small the deviation of the switch is from the ideal step function H. In this sense, no approximation of the switch can be considered a reliable model of the large-scale behaviour, as it will be sensitive to parameter variations of size $\varepsilon \to 0$. Similar results obviously then hold for more than two switches.

It is important to remember that this sensitivity is not an accident of the small-scale processes (i.e. time-stepping and delay) that leads here to the particular expression (2), we take this only as it provides an example that can be explored explicitly. Similar behaviour appears to be typical of the many other possible processes as shown in [18], as we discuss in section 6.

Each of the results above is derived in what follows. In section 2 we derive the map (2) from the system (1) when subject to discretisation and delay. The map takes a range of topologies introduced in section 3, resulting in sensitivity, that is, different behaviours of the map that remain distinct as we shrink the discretisation step and delay to zero (i.e. a singular limit)L. In section 4 we show that this variability is revealed in the transition counts between modes, and occurs similarly in a system with two switches. We show in section 5 why this variability remains hidden for a one-switch system, but becomes observable with two (or more) switches. A short discussion of how this extends to other models of a switching process is given in section 6. Some closing remarks in section 7 discuss further the concepts of transition counts, and what we mean by 'sensitivity' to parameters.

2 A single switch in discrete time with delay

Consider a variable $x \in \mathbb{R}$, whose rate of change $\dot{x}$ switches between values $A(x)$ for $x < 0$ and $B(x)$ for $x > 0$. This could represent the control variable of a multi-variate problem $(\dot{x}, \dot{y}, \dot{z}, ...)$, but let us concern ourselves only with x for now.

We are only interested in behaviour local to the switch, so let us expand (3) about $x = 0$ as

$$\dot{x} = a - (a + b)\, H(x) \; + \; g(x) \tag{5}$$

where $a = A(0)$ and $b = B(0)$ represent the two possible values of $\dot{x}$ across the switch, while $g(0) = 0$.

This is an idealised mathematical expression, and its solutions simply evolve towards $x = 0$ in finite time. What is the effect of adding small-scale non-idealities that attempt to model a real physical system or a numerical simulation? This can lead to surprisingly intricate and unpredictable behaviour, as demonstrated in [18], and here we are able to show explicitly how this arises by considering two analytically tractable non-idealities: discretisation and delay. We discuss what is known about other non-idealities in section 6, and show in particular that discretisation with hysteresis leads to similar expressions to what follows.

To begin, taking (5), introduce a small time-delay σ in the switch by writing

$$\dot{x}(t) = a - (a + b)H(x(t - \sigma)) + g(x(t - \sigma)) \; . \tag{6}$$

Then discretise the time variable in fixed steps $\delta t = \varepsilon$, for some small positive ε, and let $\sigma = \varepsilon\tau$ for some integer τ. Rescaling with

$$\phi = \frac{b}{a} \; , \qquad u = \frac{x}{\varepsilon a} \; , \tag{7}$$

we obtain the map

$$u_{n+1} = \begin{cases} f_1(u_n) = u_n - \phi & \text{if} \quad u_{n-\tau} > 0 \; , \\ f_0(u_n) = u_n + 1 & \text{if} \quad u_{n-\tau} < 0 \; . \end{cases} \tag{8}$$

We could prescribe a value u_{n+1} at $u_{n-\tau} = 0$, but it is enough here to let $u_{n+1} \in [f_0(0), f_1(0)]]$; in what follows in this section, $u = 0$ will just provide a boundary point between appliying f_0 or f_1. For simplicity we neglect the non-local term g, which adds a correction to (8) only of size εu and would not qualitatively alter the results, but would prevent the explicit analysis

that follows. The local map (8) is sufficient for our purposes, and in section 4 we use its outcomes to develop a more general numerical approach.

Due to the delay, the map (8) is time-dependent, but we can obtain an autonomous form. The system switches between $\varepsilon\dot{u} = 1$ and $\varepsilon\dot{u} = -\phi$ either side of the switching threshold $u = 0$. Solutions evolve in time-steps $\delta t = \varepsilon$, indexed by n. Each switch is activated after passing $u = 0$ with a delay of τ time-steps, causing trajectories of (8) to change from leftward to rightward motion, and vice versa, in regions D_0 and D_1 respectively, defined by

$$D_1 = (\ \tau\ ,\ \tau + 1\ )\ , \tag{9a}$$

$$D_0 = (\ -(\tau + 1)\phi\ ,\ -\tau\phi\ )\ . \tag{9b}$$

Let δD_i denote the boundary of D_i. Since solutions of (8) simply travel back and forth between D_1 and D_0, we can restrict our attention to just one of them. To find the map from D_1 to itself, compose k steps of the 'leftward' map $u_{n+1} = u_n - \phi$ with j steps of the 'rightward' map $u_{n+1} = u_n + 1$, giving

$$u_{n+k+j} = u_n - k\phi + j\ , \qquad u_n \in D_1\ . \tag{10}$$

The values of k and j are determined by taking an initial condition $u_n \in D_1$, letting this travel to a point $u_{n+k} \in D_0$, which implies the condition $-\phi(\tau + 1) < u_n - k\phi < -\phi\tau$. This then returns to a point $u_{n+j+k} \in D_1$, implying $\tau < u_n - k\phi + j < \tau + 1$. Since τ is also an integer these inequalities can be rearranged into

$$k = \left\lceil \tau + \frac{u_n}{\phi} \right\rceil \qquad \& \qquad j = \lceil k\phi + \tau - u_n \rceil\ , \tag{11}$$

where $\lceil z \rceil$ denotes the smallest integer such that $z \leq \lceil z \rceil$. These 'ceiling' functions in (11) cause the topology of the map to change with ϕ and τ, and to change rapidly with τ when ϕ is small. Note that (10) and (11) are independent of ε, so any results we find concerning the topology and dynamics of this map in section 3 persist in the limit $\varepsilon \to 0$.

The same map is obtained if we discretise before introducing delay, i.e. the ordering of our arguments above does not matter. Despite the simplicity of the system we started with in section 2, this ε-perturbed model reveals surprisingly intricate dynamics.

3 The many topologies of the 1D map

The map (10) has discontinuities at u-values where the ceiling functions in (11) change value, leading to jumps in the values of k and/or j. According

to (11), the value of k jumps where

$$\tau + \frac{u}{\phi} = N_k \in \mathbb{N} \tag{12a}$$

and the value of j jumps where

$$k\phi + \tau - u = N_j \in \mathbb{N}\,. \tag{12b}$$

The corresponding discontinuities in the map (10) occur at $u = U_k$ or $u = U_j$ which we define as

$$U_k = (N_k - \tau)\phi \qquad \text{or} \qquad U_j = k\phi - N_j + \tau \tag{13}$$

for $N_j, N_k \in \mathbb{N}$. The map exhibits different topologies in the parameter space of (τ, ϕ) as the discontinuities (13) move in and out of the interval D_1. In particular, the topology changes at bifurcation curves in (τ, ϕ) space when:

1. A discontinuity U_k lies on a boundary of D_1, i.e. $U_k \in \delta D_1$. The bifurcation curves can be calculated by substituting $u = \tau$ or $u = \tau + 1$ into (12a), giving

$$\tau + \frac{\tau}{\phi} \in \mathbb{N} \qquad \text{or} \qquad \tau + \frac{1+\tau}{\phi} \in \mathbb{N}\,. \tag{14}$$

2. A discontinuity U_j lies on a boundary of D_1, i.e. $U_j \in \delta D_1$. The bifurcation curves can be calculated by substituting $u = \tau$ or $u = \tau + 1$ into (12b), giving

$$k\phi \in \mathbb{N}\,. \tag{15}$$

3. A discontinuity maps under (10) to a boundary of D_1, i.e. $u = U_k \mapsto \delta D_1$, where $u_n - k\phi + j = \{\tau \text{ or } \tau + 1\}$. The bifurcation curves can be calculated by substituting $u_n = \{k\phi - j + \tau \text{ or } k\phi - j + \tau + 1\}$ into (12a), giving

$$k + \tau + \frac{\tau - j}{\phi} \in \mathbb{N} \qquad \text{or} \qquad k + \tau + \frac{\tau - j + 1}{\phi} \in \mathbb{N}\,. \tag{16}$$

Note that there are no similar curves associated with $u = U_j \mapsto \delta D_1$ as the analogous equations turn out to be trivial.

These conditions define a diagram of different map topologies over the space of (τ, ϕ) that is somewhat intricate, but importantly is ε-independent, and hence retains its intricate dependence on the τ and ϕ parameters as $\varepsilon \to 0$. The diagrams are constructed by plotting the curves that satisfy the above conditions, subject to the values of (τ, ϕ, k, j) giving valid values of $U_k, U_j \in D_1$ and $U_k \mapsto u \in D_1$ according to (10)-(11). We describe the map topologies below for $\phi > 1$ and $\phi < 1$ separately.

3.1 The case $\phi > 1$

In each region of (τ, ϕ) space the map takes different sets of k and j values. For $\phi > 1$ these fall into just a few topological types, illustrated in fig. 1, and defined as:

0. $j = k\phi$, the map has one or two jumps and is the identity on a subset of D_1, or has no jumps and is the identity on the whole of D_1.
1. The map is a circle homeomorphism with one jump at some $u = U_j$.
2. The map is injective with one jump at some $u = U_k$.
3. The map has two jumps at some $u = U_j$ and $u = U_k$.
4. The map has two jumps at different $u = U_k$ values.
5. The map has three jumps, one at some $u = U_k$ and two at different $u = U_j$ values.

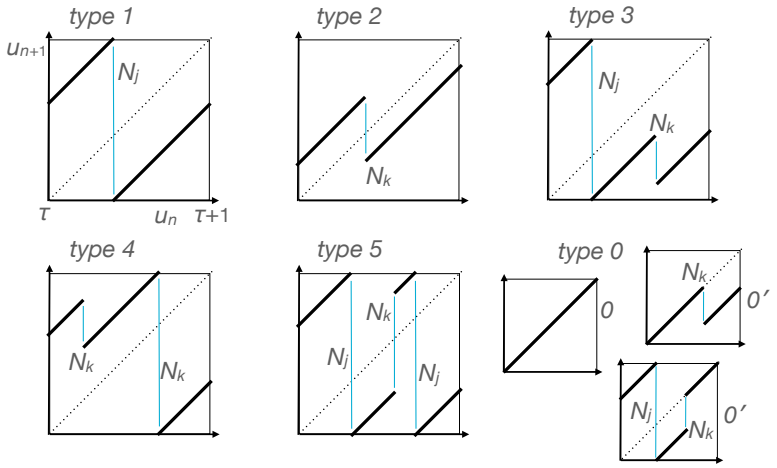

Figure 1: The 5 typical topologies of the map, plus the degenerate type 0. The types are distinguished by the number of jumps N_j where j changes value, and N_k where both j and k both change value, according to (11) and with N_j, N_k, defined in (13). In type 0 the map is the identity over all or part of $D_1 = (\tau, \tau + 1)$, labelled as types 0 or $0'$, respectively.

The regions of the (ϕ, τ) plane where the map takes each topology are shown in fig. 2, with a close up of a typical region in fig. 3. The bifurcation curves between topologies are given by (14)-(16). In fig. 2 and fig. 3, the horizontal line segments are given by the condition (15), while the curves with

positive gradient are given by (14), and the curves with negative gradient are given by (16) (more easily seen in fig. 3).

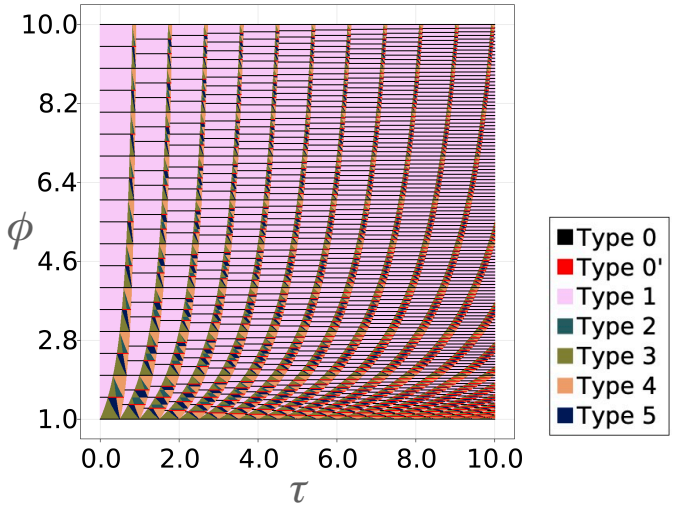

Figure 2: Bifurcation diagram of the map's topological types. Figure 3 shows a magnification and more detailed description.

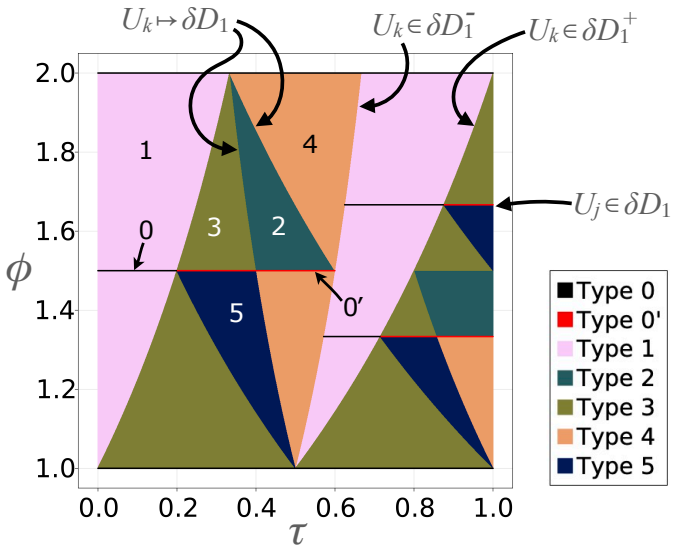

Figure 3: Magnification of the lower-left corner of fig. 2. δD_1^+ and δD_1^- denote the upper and lower boundaries of D_1 (i.e. $\delta D_1^- = \tau$ and $\delta D_1^+ = \tau + 1$).

Each pink 'tongue' (where the map has type 1) has a unique k value,

bounded by the curves (14) where $U_k \in \delta D_1^{\pm}$. The value of j jumps at the horizontal lines (15) where $U_j \in \delta D_1$, on which the map has type 0 inside the pink tongues and type $0'$ in the strips between tongues. The strips are partitioned into 3 sided tiles of types 2-5 by the curves (16) where $U_k \mapsto \delta D_1$.

Note that fig. 2-3 are plotted in continuous variables (τ, ϕ) for clarity, but τ is actually an integer in the system above, and so the map only exists on slices $\tau \in \mathbb{N}$ taken through these figures.

3.2 The case $\phi < 1$

For $\phi < 1$ the curves from fig. 2 continue in a fairly simple manner, but the topologies between them fall into an infinite number of different classes, with different numbers of branches that grow as $1/\phi$. This happens because the righthand set D_1 is a factor $1/\phi$ smaller than the lefthand set D_0, and so maps into D_0 under multiple (roughly $1/k$) different values of leftward steps k, with each different k giving a different map branch.

The classification above can still be applied, subject to a mapping that relates the dynamics of the map on D_0 for $\phi < 1$ to the map on D_1 for $\phi > 1$. More precisely, the coordinate change $(u, \phi) \mapsto (-u\phi, 1/\phi)$ converts the map in the u-coordinate on $u \in D_0 = (-\phi(\tau+1), -\phi\tau)$ with $\phi < 1$, to a map in the z-coordinate on $z \in D_0' = (-(\tau+1), -\tau)$ with $\psi > 1$.

This means that the bifurcation diagram in $(\tau, \phi) \in \mathbb{R}^+ \times [0, 1]$ is just the same as $(\tau, \phi) \in \mathbb{R}^+ \times [1, \infty)$, only inverted around $\phi = 1$ under the mapping $\phi \to 1/\phi$, making the types infinitely crowded towards $\phi \to 0$. The resulting diagram of topological types of the map is shown in fig. 4.

The outcome for both $\phi > 1$ and $\phi < 1$ is that changing τ or ϕ results in changes in the map topology. Consider any fixed value of ϕ, for instance. The bounding curves in fig. 2-fig. 4, given by conditions (14), have asymptotes at each integer τ, meaning that any change in the number of steps τ in the delay results in a different map topology. No matter how small we make the time-step $\Delta t = \varepsilon$ and the actual time delay $\sigma = \varepsilon\tau$, this variation with the value of τ remains.

3.3 Dynamics of the 1D map

The map (8) for the time-delayed discrete system is piecewise-linear, and almost every solution eventually reaches the region D_1, where its future trajectory is described by the map (10). (The 'almost' here means all orbits that have at least one iterate in D_0 and D_1 or beyond them, i.e. away from

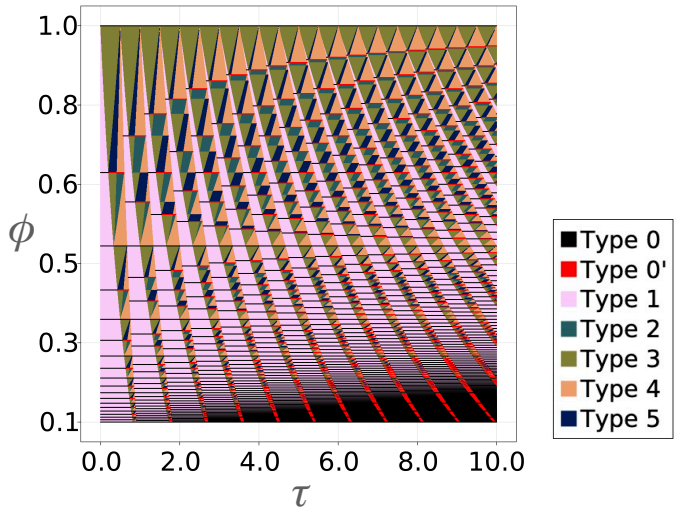

Figure 4: Bifurcation diagram of the map's topological types extending fig. 2 to $\phi < 1$. The 'Type' refers to the corresponding class in fig. 2 under the mapping $(u, \phi) \mapsto (-u\phi, 1/\phi)$.

the switching threshold, excluding some peculiar initial conditions that can give orbits that live for all time in the interval between D_0 and D_1 due to the delay, which are outside our present interest.)

Even within any one of the topological classes above, the dynamics of such piecewise continuous maps is known to be highly complex. Each class is an example of an *interval translation map*, which have an extensive literature in themselves, see [23, 5] for general results and references. Let us summarise just a few qualitative aspects here for illustration.

The system exhibits different behaviours depending on the parameter ϕ. If ϕ is irrational then the map displays dense quasiperiodic orbits or multi-band chaotic attractors. If ϕ is rational, the orbit of any point is eventually periodic. In fig. 5, the largest period of the attractor in the map is plotted in the (τ, ϕ) plane, obtained through simulations of (10). The locations of the underlying topological tongues fig. 2 are clear, with further complexity within them.

In piecewise-linear maps with a single discontinuity, the parameter ϕ determines a winding number that governs the periodicity of the map. In the case of multiple and changing numbers of discontinuities, as we have here, the situation is more complex and there is no obvious definition of the winding number. Nevertheless, the parameter ϕ still strongly influences the period of the attractor, see e.g. [3], as evident in the right-hand picture

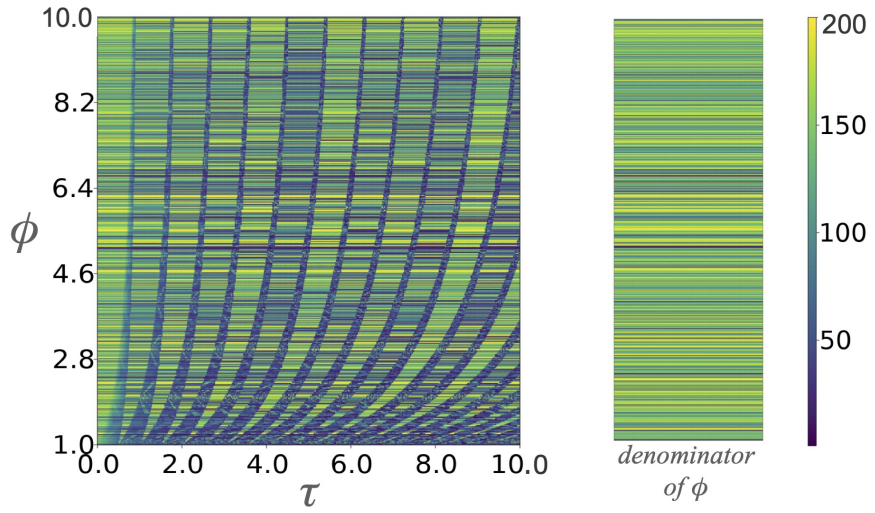

Figure 5: Left: largest period of the map (10) plotted for rational values of ϕ (period indicated by colour). Right: corresponding plot of the denominator of $\phi = p/q$.

of fig. 5. In this picture, the denominator of ϕ is shown for rational values of ϕ represented as $\phi = p/q$, where p and q are the minimal values of the numerator and denominator, respectively. The denominator of ϕ generates distinct horizontal stripes in the periodicity plot (left-hand picture of fig. 5), which overlays the topological tongues from fig. 2. These horizontal stripes represent different periods associated with various rational values of ϕ.

However, the bifurcation diagram is even more intricate still, containing many other structures beyond the tongues and horizontal stripes, some of which are magnified and shown in fig. 6.

Hence the dynamics of the map (10) is dependent on a combination of the intricate bifurcations of piecewise-linear maps and the already complex topologies from fig. 2.

The intricacy of these maps is such that plots of periodicity, such as fig. 5-fig. 6, can be misleading due to the computational necessity of plotting rational values of ϕ. The maximum period is bounded by the denominator of ϕ for rational values and is infinite for irrational values. Thus, the precise patterns observed in fig. 5 are strongly influenced by the method used to sample ϕ, for instance whether we take a particular subset of rational ϕ values or select values randomly, as briefly illustrated in appendix A.

In deriving (10) we neglected higher order terms, so the results above describe the leading order approximation of a typical system (5) around a switching threshold. Higher order corrections would perturb the map, the

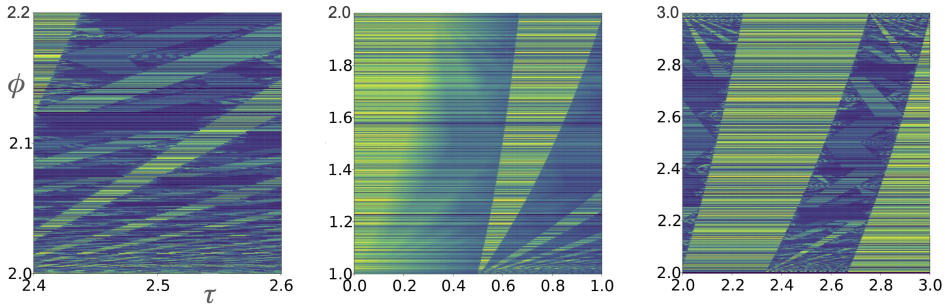

Figure 6: Magnifications of fig. 5 showing intricate features of the bifurcation structure.

lowest order corrections giving it a gradient different from one, but simulations not included here confirm similar parameter dependence when higher order terms are included. The dynamics of such maps are well understood if they have a single discontinuity, i.e. types 1 and 2. Comprehensive classifications are given in [3], which present a complex picture of multi-band chaotic, quasiperiodic and periodic attractors, and these go through band-count and period-incrementing or accumulation cascades under variation of parameters. However, since the map has gradient one (or close to one with non-local corrections) almost everywhere, we are in a very degenerate case, similar to the point $a_R = a_L = 1$ of the bifurcation diagram in Fig. 6.24 of [3]. Less is known about maps with multiple discontinuities, and they exhibit bifurcation phenomena that have only begun to be explored, see e.g. [34]. The invariants of maps with multiple discontinuities have been studied in the context of interval translation maps [23, 5]. The novelty of the map (10) in our context is that not only does the dynamics of the map depend intricately on parameters, but so does the basic topology of the map itself, such as its number of discontinuities. The crucial point, however, is that all of this intricacy remains as $\varepsilon \to 0$.

4 Transition counts

We have seen above how a simple switching between modes varies with parameters in the presence of discretisation and delay. For this simple case the variation can be described explicitly by the map (2).

Such explicit results cannot be generalised to systems with multiple switches, or if we introduce further switching processes other than discretization and delay, such as hysteresis or stochasticity, each of which in isolation

are also known to have complex dependence on parameters, see e.g. [18].

Rather than looking explicitly at the dynamics and its attractors, let us concern ourselves with the amount of time the system spends in either of its modes, because this will determine larger-scale observable behaviour, as we will show in section 5. Alternatively we can count how many times the system switches from one mode to another, in either direction.

There is good reason for looking closely at both of these two quantities: the *time proportions* in each mode and the *transition counts* between them. As we shall see, they reveal different features of the behaviour, with *transition counts* revealing variability as we show here in section 4, while *time proportions* reveal its large-scale consequences as we show in section 5. Both quantities have the benefit of being easily extendable to systems where the kind of analysis in the preceding sections is not possible, such as systems with multiple switches, and perhaps where different switches involve different small-scale transitions processes, of the kind we discuss briefly in section 6. Finally, each relate to wider literature in different ways, as we discuss in section 7.

First we will look first at transition counts in this section, using them to reveal numerically how the variability of the one-switch system found above, extends to a system with two switches.

4.1 Transition counts for one switch

Take the one-dimensional system (5), approximated by the map (8). At each time instant the map

$$u_{n+1} = f_i(u_n) \qquad \text{with} \qquad i = H(u_{n-\tau})$$

is applied, using the functions f_i given in (8). Hence the map is a discrete-time process iterating between the two modes $i = 0$ and $i = 1$, as illustrated in fig. 7.

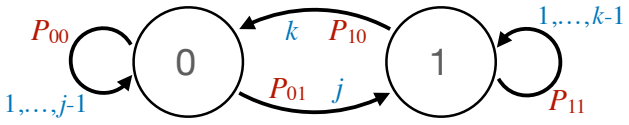

Figure 7: Representation of the one-switch system as a chain, showing the two modes 0 and 1, the transition counts P_{nm} between them, and the numbers of steps along them.

Let us identify the mode $i = 0, 1$, in the n^{th} time step as

$$m_n = H(u_{n-\tau}) \,, \tag{17}$$

and define a 2×2 matrix that counts transitions from mode h to mode i, over N time-steps,, with components

$$P_{hi} = \frac{\#\{\ (m_n, m_{n+1}) = (h, i)\ \text{ for } n = 1, ..., N-1\ \}}{N}\ , \tag{18}$$

i.e. the number of steps in a trajectory for which $m_{n+1} = i$ and $m_n = h$, divided by the total number of steps. This matrix is computed numerically in fig. 8, by iterating the map (8) for a sufficiently long time that the values of (18) converge. The value plotted in fig. 8 is the spectral gap $\lambda_1 - \lambda_2$, where $\lambda_1 = 1 > \lambda_2$ are the eigenvalues of P_{hi}. (We should note that the map here does not represent a Markov process, so the usual results relating the spectral gap to the mixing time of the system do not hold here, but we make further remarks on this in section 7).

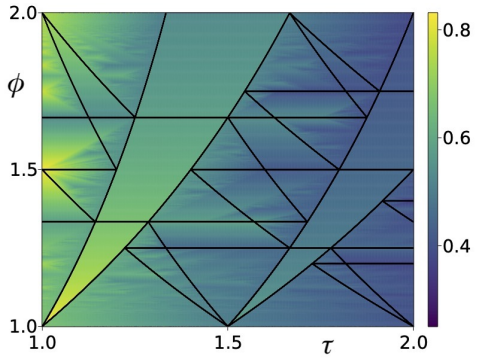

Figure 8: Spectral gap of the transition count matrix (18), in the (τ, ϕ) plane corresponding to fig. 3. The colour map indicates the value of the spectral gap (scale given on the right).

In each simulation, a random initial u value is chosen, and the system is run for 10^5 time-steps δt to calculate the components P_{hi}, hence $T = 10^5 \delta t$. For completeness, one could average over multiple simulations with different initial values over $u \in D_1$, however we find that the results are similar, while being far more computationally expensive.

The extent of variability is shown by zooming in on portions of fig. 8, as in fig. 9. The transition counts evidently reflect the topology of the underlying map (with the black curves in fig. 8 being copied from fig. 2).

Extremely fine-scale structure found around a type 0 boundary is shown in fig. 10. At this magnification the pattern is also affected by the choice of initial conditions: the top row of fig. 10 used a fixed initial condition, the bottom row used a random initial condition for each point. (This effect of the initial conditions does not have a visible effect on fig. 8-fig. 9.)

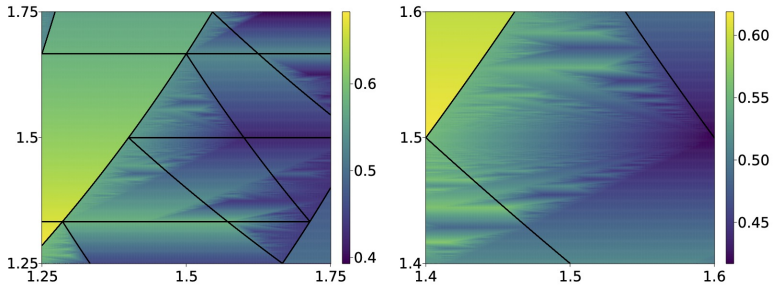

Figure 9: Magnifications of some of the detail from fig. 8.

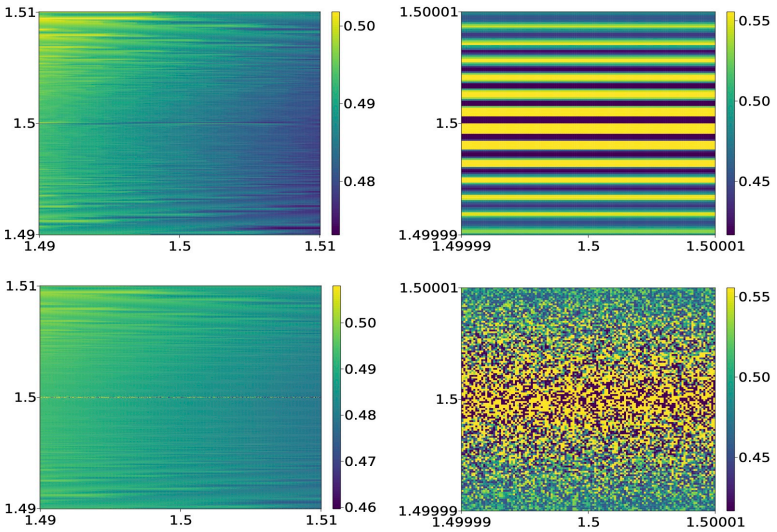

Figure 10: Further magnifications of fig. 8 around a class 0 boundary at $\phi = 1.5$ reveal extreme intricacy in the transition counts. Top: simulated using a fixed initial point $u_0 = 10^{-4}$. Bottom: simulated with random initial point u_0.

Notably these transition counts reveal (though they do not explain) the dependence of the dynamics on τ and ϕ, without requiring the detailed modeling and analysis of the switching process itself, as was required to produce fig. 2-fig. 4, and without the sampling issues of fig. 5. Future work will look more into the structure of P_{hi} and its relation to invariants of the dynamics (and we make some further remarks on it in section 7), but it is sufficient for our purposes here that this permits us to extend these results, numerically, to a system with two switches, for which such explicit analysis is not yet known.

4.2 Transition counts for two switches

Let us define a system similar to (5) but with two switches. Consider two independent variables, x_1 and x_2, each governed by an equation similar to (1), say $\dot{x}_i = a_i - (a_i + b_i)H(x_i)$ for $i = 1, 2$, with $a_i, b_i > 0$. Let us divide each through by a_i and re-label the scaled variable x_i/a_i simply as a_i, to give

$$\begin{aligned} \dot{x}_1 &= 1 - (1 + \phi_1)H(x_1) \ , \\ \dot{x}_2 &= 1 - (1 + \phi_2)H(x_2) \ . \end{aligned}$$

Each of these is described by maps identical to the earlier one-dimensional system, giving us nothing new, so let us couple them by introducing a switch $H(x_1)$ in the $\dot{x}_2$ equation and vice versa. Purely for simplicity (one may consider other such coupling terms), we will take the same term on each line,

$$\begin{aligned} \dot{x}_1 &= 1 - (1 + \phi_1)H(x_1) - \phi_3 H(x_1)H(x_2) \ , \\ \dot{x}_2 &= 1 - (1 + \phi_2)H(x_2) - \phi_3 H(x_1)H(x_2) \ , \end{aligned} \tag{19}$$

in terms of the Heaviside step functions $H(x_i)$. Denote the four modes on the righthand-side of (19) as $F_{v_1 v_2}$, that is,

$$(\dot{x}_1, \dot{x}_2) = F_{v_1 v_2} \quad \text{where} \quad v_i = H(x_i) \ , \tag{20}$$

labelled by the index pairs $(v_1 v_2) \in \{00, 01, 10, 11\}$, such that

$$\begin{aligned} F_{01} &= (1, -\phi_2) \ , \qquad & F_{00} &= (1, 1) \ , \\ F_{10} &= (-\phi_1, 1) \ , \qquad & F_{11} &= -(\phi_1 + \phi_3, \phi_2 + \phi_3) \ . \end{aligned} \tag{21}$$

Hence setting all $\phi_i > 0$ ensures that in each mode the system evolves towards the switching thresholds $x_1 = 0$ and $x_2 = 0$. One may consider more general expressions, this will be sufficient to illustrate our central result (for more general expressions see [17, 18]).

Let us then discretise the system and impose a delay across the switch, following a procedure similar to (5). Let switching occur with delays σ_i across each threshold $x_i = 0$, so that the mode is given by $v_i = H(x_i(t - \sigma_i))$ for some small $\sigma_1, \sigma_2 \in \mathbb{R}$. Then introduce a discretisation into time-steps $\delta t = \varepsilon$, and write the discretised variables as $x_{i,n}$. Finally let $\sigma_i = \varepsilon \tau_i$ for some $\tau_1, \tau_2 \in \mathbb{N}$, to obtain the system

$$\begin{aligned} &(x_{1,n+1}, x_{2,n+1}) = (x_{1,n}, x_{2,n}) + \varepsilon F_{v_1 v_2} \\ &\text{where} \quad v_i = H(x_{i,n-\tau_i}) \ , \end{aligned} \tag{22}$$

with the four modes $F_{v_1 v_2}$ given by (21).

An explicit autonomous form for this map is not yet known (unlike the one-switch system which led to the explicit map (2)). Indeed, such a closed form may not be possible for two switches, and at least such a map could not be unique in forward time, because at any given instant a state may possess different histories of switches yet to run their course. That is, when a solution reaches $x_2 = 0$, say, it may or may not be waiting the τ_1 time-steps needed for a switch across $x_1 = 0$ to be carried out, or vice versa, so the system evolution is always dependent on its history, and is not determined by its present state.

Instead, let us use the system's transition counts to show that, similar to the one-switch system, this depends on the system parameters in a manner that will not vanish as $\varepsilon \to 0$. The system's representation as a chain is shown in fig. 11. At any given point (x_1, x_2) in a mode $v_1 v_2$, the system can remain in the same mode, or switch into one of the other three. One may find similar representations of a discrete-delayed genetic regulatory network in [7].

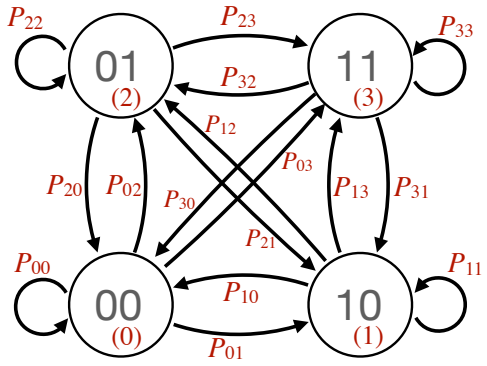

Figure 11: Representation of the two-switch system as a chain. Each node shows the binary $v_1 v_2$ index, with the index m in brackets, and the transition counts P_{mn} between then.

It is convenient to re-number the modes $\{00, 10, 01, 11\}$ as $\{1, 2, 3, 4\}$, and then identify the mode number $1, 2, 3, 4$, in the n^{th} time step as

$$m_n = H(x_{1,n-\tau_1}) + 2H(x_{2,n-\tau_2}) \; . \tag{23}$$

Similar to the one-switch system we then define a 4×4 matrix of transition counts over N time-steps with components

$$P_{hi} = \frac{\#\{\ (m_n, m_{n+1}) = (h, i)\ \text{ for } n = 1, ..., N-1\ \}}{N} \; . \tag{24}$$

From an initial condition in an ε-neighbourhood of $x_1 = x_2 = 0$, we iterate (22) over a sufficient time interval that the values of P_{hi} converge. We represent them in fig. 12 by plotting the spectral gap of the resulting 4×4 matrix, in fact here we plot the inverse of the spectral gap to improve the contrast of the image.

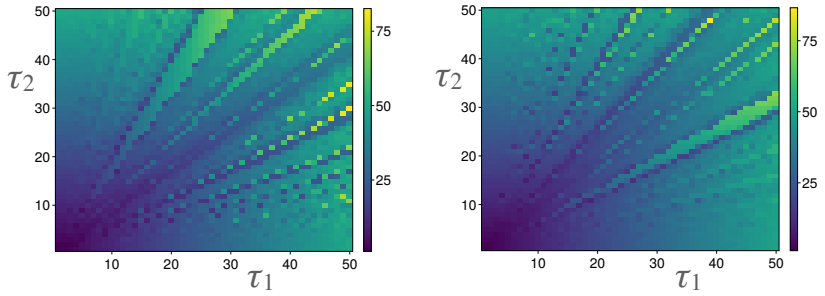

Figure 12: Plots of $1/$*spectral gap* for the two-switch system (20), with value indicated by the colour map (scale given on the right). Left: $\phi_1 = 33/7$, $\phi_2 = 7/5$, $\phi_3 = 10/9$. Right: $\phi_1 = 31/15$, $\phi_2 = 180/37$, $\phi_3 = 35/29$. Note that these plots are pixelated because they are calculated at discrete τ values (since we no longer have an explicit map we cannot plot in continuous τ as we could in fig. 8).

The spectral gap varies with the two parameters τ_i, and since the time-delays are $\sigma_i = \varepsilon\tau_i$, and the time-step is ε, this variation remains if we take $\varepsilon \to 0$ to make the delay and time-step infinitesimally small. Similar variation can be seen by plotting against the parameters ϕ_i.

Future work will look more into the use of these transition counts to characterise the dynamics in more detail, and particularly how different switching process results in different transition count diagrams. To this end we briefly summarise what is known about such processes, and how they relate to the results above, in section 6.

Our real interest is not actually in these local transitions themselves across the switching thresholds, but rather in the fact that they determine large-scale so-called *sliding* dynamics, which occurs when such switching across $x = 0$ (or $x_1 = 0$ and $x_2 = 0$) affects some additional variable. We turn to this in the next section.

5 Fine-scale process and large-scale sliding

When a solution in a nonsmooth system encounters a switching threshold, it might simply cross through the threshold, therefore encountering it only fleetingly. The systems (5) and (19) model the more interesting situation

in which solutions become constrained to move along a switching threshold, commonly referred to as *sliding*, following [10, 11, 31, 25]. Let us look at how the dynamics observed above, in the motion *across* the switching threshold (in an ε-neighbourhood of $x = 0$), affects motion *along* the switching threshold (along $x = 0$) during sliding. We do this first for a system with one switch, then a system with two.

5.1 Sliding with one switch

Let us revisit the one-switch system (5), with equation $\dot{x} = a - (a+b)H(x)$, from the perspective of a Filippov system, and examine how this relates to the dynamics of the map (2), that is, $x \mapsto x + \varepsilon(aj - bk)$, around $x = 0$.

Consider a system of variables (x, y), and a switch that depends only on x, given by

$$\begin{aligned} \dot{x} &= a - (a+b)H(x) \ , \\ \dot{y} &= A + (B - A)H(x) \ . \end{aligned} \tag{25}$$

Here, y is a vector variable, and A and B represent vector fields (which may be functions of x and y, but this is not critical for our analysis).

In the Filippov formalism, when a system switches repeatedly across $x = 0$, the times spent in the regions $x > 0$ and $x < 0$ are used to determine an aggregate *sliding* dynamics that approximates the motion along $x = 0$. This sliding motion is also known as Utkin's *equivalent control* [10, 27]. The standard argument is as follows.

If, over some time interval, the system spends a proportion μ of its time evolving according to the $x > 0$ system $\dot{x} = -b$, and the remaining portion $1-\mu$ evolving according to the $x < 0$ system $\dot{x} = +a$, then its overall motion can be expressed as

$$\begin{aligned} \dot{x} &= -b\mu + a(1 - \mu) \ , \\ \dot{y} &= B\mu + A(1 - \mu) \ , \end{aligned} \tag{26}$$

letting

$$\mu \in \begin{cases} H(x) & \text{if } \ x \neq 0 \ , \\ [0, 1] & \text{if } \ x = 0 \ . \end{cases} \tag{27}$$

Since a and b are positive, this aggregate motion eventually becomes constrained to $x = 0$, from which we can infer that the system must satisfy the

constraint $\dot{x} = 0$. Using (26) with $\dot{x} = 0$, we find that μ takes the value

$$\mu = \frac{1}{1+\phi} \,, \tag{28}$$

where $\phi = b/a$. Upon substituting the value of μ from (28) back into (25), we obtain the sliding dynamics along $x = 0$ as

$$\begin{aligned} \dot{x} &= 0 \,, \\ \dot{y} &= A + (B - A)\frac{1}{1+\phi} \,. \end{aligned} \tag{29}$$

The sliding dynamics described by (29) represents a well-determined, if idealised, motion along an infinitesimal neighbourhood of $x = 0$. There are limited results studying how well this approximates less idealised switching processes. Here, let us use the explicit map for the discrete-delay process to see how well it is approximated by (29), and we discuss some other processes in section 6.

To do this, we calculate the proportions of time the system spends in either of its two modes. In the neighbourhood of the switching threshold, the system (5) evolves in time-steps of size ε, with a delay $\sigma = \varepsilon\tau$, according to the map $x_{n+k+j} = x_n + \varepsilon(j - k\phi)$. This map evolves from the region D_1, across the switch and then back again to D_1. In x-space, D_1 corresponds to the region $\varepsilon\tau < x < \varepsilon(1+\tau)$, ensuring that the dynamics remain in an ε-neighbourhood of the switch, consistent with (29) as $\varepsilon \to 0$. We then wish to know how y evolves during this process.

The integers k and j conveniently count the time increments in each mode. Consider an orbit that has returned to D_1 multiple times. Let the total number of rightward and leftward steps be K and J, respectively. Then, u_{n+K+J} implies $\Delta x = x_{n+K+J} - x_n = \varepsilon(J - K\phi) \in \varepsilon[-1, 1]$. The proportion of time spent evolving in the leftward mode can thus be written as

$$\hat{\mu} = \frac{K}{J+K} = \frac{1}{1+\frac{J}{K}} = \frac{1}{1+\phi+\frac{\Delta x/\varepsilon}{K}} = \frac{1}{1+\phi} + \mathcal{O}\left(\frac{1}{K}\right) \,, \tag{30}$$

hence

$$\begin{aligned} \dot{x} &= \mathcal{O}\left(\varepsilon\right) \,, \\ \dot{y} &= A + (B - A)\frac{1}{1+\phi} + \mathcal{O}\left(\frac{1}{K}\right) \,. \end{aligned} \tag{31}$$

This implies that, despite the variability of the left-right switching resulting from the map (10), the large-scale motion remains approximately consistent with Filippov dynamics for sufficiently long times K. This, of course, is the basic premise of Filippov and Utkin's legacy on sliding modes [10, 27]. In the next section, we will show that this error ceases to be small for a system with multiple switches.

There are situations where non-Filippov dynamics can occur at one switch due to novel 'hidden' terms, see [17, 18, 21], and indeed these were long recognised by both Filippov and Utkin (see classic counter-examples to the sliding formalism in [10, 27, 21]), but these are beyond our scope here. A similar result to (31) hold for a system with hysteresis (in place of discretisation and delay), as can be found in [4].

5.2 Sliding with two switches

Let us derive the corresponding results to section 5.1 for the two-switch system (19). We shall see that the sliding dynamics is then indeterminate, allowing the kind of variation seen in fig. 8 to affect the large-scale dynamics.

First consider x_1 and x_2 to inhabit a larger state space (x_1, x_2, y) for some vector variable y, and extend (20) to

$$(\dot{x}_1, \dot{x}_2, \dot{y}) = F_{v_1 v_2} \quad \text{where} \quad v_i = H(x_i) \ , \tag{32}$$

with modes

$$\begin{aligned} F_{01} &= (1, -\phi_2, C_{01}) \ , \qquad & F_{00} &= (1, 1, C_{00}) \ , \\ F_{10} &= (-\phi_1, 1, C_{10}) \ , \qquad & F_{11} &= -(\phi_1 + \phi_3, \phi_2 + \phi_3, C_{11}) \ . \end{aligned} \tag{33}$$

In terms of the Heaviside step function H we can write this as

$$\begin{aligned} \dot{x}_1 &= 1 - (1 + \phi_1)H(x_1) - \phi_3 H(x_1)H(x_2) \ , \\ \dot{x}_2 &= 1 - (1 + \phi_2)H(x_2) - \phi_3 H(x_1)H(x_2) \ , \\ \dot{y} &= C_{00} + (C_{10} - C_{00})H(x_1) + (C_{01} - C_{00})H(x_2) \\ &\qquad + (C_{11} + C_{00} - C_{10} - C_{01})H(x_1)H(x_2) \ . \end{aligned}$$

The C_{ij} extend the vectors A, B, from the one-switch system, and similar to the previous section, we are not concerned with the precise nature of these (which could be functions of (x_1, x_2, y)). Our aim is to approximate the aggregate motion of this system over an extended interval of time when its motion is constrained to the switching threshold $x_1 = x_2 = 0$. To find this,

let $\mu_{v_1v_2}$ represent the proportion of time that the system evolves according to the mode $v_1v_2 \in \{00, 10, 01, 11\}$. The system can then be described by

$$\begin{aligned} \dot{x}_1 &= \mu_{00} - \mu_{11}(\phi_1 + \phi_3) - \mu_{10}\phi_1 + \mu_{01} \ , \\ \dot{x}_2 &= \mu_{00} - \mu_{11}(\phi_2 + \phi_3) + \mu_{10} - \mu_{01}\phi_2 \ , \\ \dot{y} &= \mu_{00}C_{00} + \mu_{11}C_{11} + \mu_{10}C_{10} + \mu_{01}C_{01} \ , \end{aligned} \tag{34}$$

where

$$\mu_{ij} \in [0, 1] \ . \tag{35}$$

Since the $\mu_{v_1v_2}$ are proportions of time they must sum to unity, so

$$\mu_{00} + \mu_{01} + \mu_{10} + \mu_{11} = 1 \ . \tag{36}$$

Motion along either one of the thresholds $x_1 = 0$ (with $x_2 \neq 0$) or $x_2 = 0$ (with $x_1 \neq 0$) will follow equations similar to those in the previous section. Let us look instead at what happens if motion becomes constrained to the intersection of the two switching thresholds, where $x_1 = x_2 = 0$ and $\dot{x}_1 = \dot{x}_2 = 0$. Then the motion satisfies $(\dot{x}_1, \dot{x}_2) = (0, 0)$, and these constraints, along with (36), allow us to express three of the time proportions all in terms of μ_{11},

$$\begin{aligned} \mu_{10} = \frac{1 - \phi_3\mu_{11}}{1 + \phi_1} - \mu_{11} \ , \qquad \mu_{01} = \frac{1 - \phi_3\mu_{11}}{1 + \phi_2} - \mu_{11} \ , \\ \text{where} \quad \mu_{11} \in [0, 1] \ , \end{aligned} \tag{37}$$

(with μ_{00} then given by (36)). In the one-switch system described earlier, the constraint of sliding along $x = 0$ provided a well-defined value (28) for the time proportion μ. Now, in the two-switch system, sliding along $x_1 = x_2 = 0$ determines the time proportions $\mu_{v_1v_2}$ only up to the set-valued relations (37). The motion along the threshold $x_1 = x_2 = 0$ is then given by

$$\begin{aligned} \dot{x}_1 = \dot{x}_2 &= 0 \ , \\ \dot{y} &= \mu_{00}C_{00} + \mu_{01}C_{01} + \mu_{10}C_{10} + \mu_{11}C_{11} \\ &= C_{00} + \hat{C}_1\frac{1}{1 + \phi_1} + \hat{C}_2\frac{1}{1 + \phi_2} + \hat{C}_3\mu_{11} \ , \\ \text{where} \quad \mu_{11} &\in [0, 1] \ , \end{aligned} \tag{38}$$

written for convenience in terms of vectors

$$\begin{aligned} \hat{C}_1 = C_{10} - C_{00} \ , \qquad \hat{C}_2 = C_{01} - C_{00} \ , \\ \hat{C}_3 = C_{11} - C_{00} - (\tfrac{\phi_3}{1+\phi_2} + 1)\hat{C}_1 - (\tfrac{\phi_3}{1+\phi_1} + 1)\hat{C}_2 \ . \end{aligned} \tag{39}$$

Hence the sliding dynamics of y along the switching threshold is set-valued, given by (38), expressed in terms of the undetermined multiplier $\mu_{11} \in [0, 1]$. This is a well-known indeterminacy of Filippov's sliding concept at intersections of switching thresholds, and many approaches have been made to resolve the resulting dynamical ambiguity, see e.g. [1, 2, 8, 16, 20, 24]. A glance at these references shows that different approaches give different outcomes, all lying among those making up the set (38), as shown in a range of numerical 'experiments' in [18]. Ultimately the value of μ_{11} can only be determined through a more detailed modeling of the switching process at the switch.

We have already noted that an explicit map cannot be obtained for the discrete-delayed system with two switches, therefore it is not possible to derive an expression for μ_{11}, or to obtain the corresponding form of (38) in the presence of discretisation and delay, as we could for one switch in (31). Instead let us calculate the unknown μ_{11}, namely the time proportion spent in the mode $v_1 v_2 = 11$, for the simulations in fig. 12. The results are shown in fig. 13. They clearly reflect the dependence on the parameters τ_i seen in the transition counts in fig. 12.

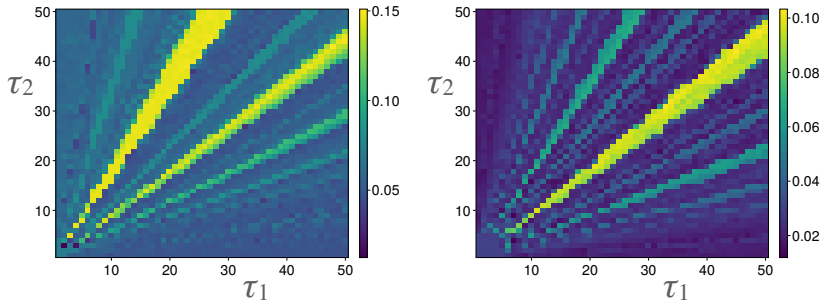

Figure 13: Simulations of the time constant μ_{11} for the two-switch system (20), in the (τ_1, τ_2) plane. This shows the variation of the dynamics with the time-delays τ_i. Left and right pictures correspond to the simulations in fig. 12. The colour map indicates the value of the time constant μ_{11} (scale given on the right).

The variability of μ_{11} with parameters is now directly observable in the sliding motion, and depends on how we model the switch, no matter how ideal (close to a Heaviside step) that switch is. To see this, let us assume in analogy to (30) that the constraint of the motion to $x_1 = \mathcal{O}(\varepsilon)$, $x_2 = \mathcal{O}(\varepsilon)$, determines the time proportions to errors of size $1/T$ over a time interval T, then the dynamics of the system (38), with discretization and delay of size

ε, obeys

$$\begin{aligned} \dot{x}_1 = \dot{x}_2 &= \mathcal{O}(\varepsilon) \ , \\ \dot{y} &= C_{00} + \hat{C}_1 \frac{1}{1+\phi_1} + \hat{C}_2 \frac{1}{1+\phi_2} + \hat{C}_3 \mu_{11} + \mathcal{O}(1/T) \ , \qquad (40) \\ \text{where} \quad \mu_{11} &\in [0,1] \ . \end{aligned}$$

Thus the variability of μ_{11} in fig. 13 directly translates into variability in the dynamics of y. Depending on the constants ϕ_i this can be arbitrarily large. This is emphasised in fig. 14, which shows two graphs plotting the value of μ_{11} for each of the two simulations in fig. 13 at a fixed $\tau_1 = 50$, and showing how this translates into variability in y. In each case we take a scalar y that obeys $\dot{y} = (1 - 10\mu_{11})C_{00}$ (using parameters given in the figure caption), for which numerically we find

$$0.1 \lesssim \mu_{11} \lesssim 0.2 \qquad \Rightarrow \qquad -0.05 C_{00} \lesssim \dot{y} \lesssim +0.1 C_{00} \ .$$

Hence $\dot{y}$ can take values that are arbitrarily large depending on the size of C_{00}, and is not even fixed in direction, as $\dot{y}$ may even change sign depending on the value of τ_2.

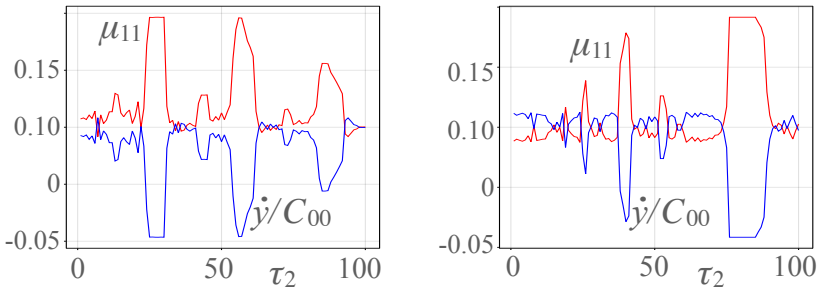

Figure 14: Graphs of the time constant μ_{11} from the plots fig. 13 with delay $\tau_1 = 50$. Also showing an example of $\dot{y}$, given by (38) with $C_{00} = C_{10} = C_{01} = -C_{11}/9$.

6 Other switching processes

The theory of dynamical systems with discontinuous switches is well established, through Filippov [10] and many works that have followed. What has not been clear in that theory is how well such models approximate less idealised switches of real world systems, *or* how reliable numerical simulations are in handling such discontinuities. Several ways of replacing discontinuous

switches with more detailed switching processes have been considered in the literature, some motivated by more precise physical modeling, others motivated by 'regularising' the switch to obtain a well-defined differential system. Below we summarise briefly what is known about dynamics involving just one switching process in isolation, or multiple interacting processes.

6.1 Isolated processes

The most popular analytic model of a switching process is via a smooth transition function. An example is the well-studied Sotomayor-Teixeira regularisation [28], which is commonly used in theoretical works (and can even be extended to deal with 'hidden' terms [26]). Smoothing is routinely used in the sigmoid switches of neural networks, and achieved in numerous ways such as elastic compliance or force interpolation in physical contact models. Theoretical results on smoothing have also been extended to multiple switches, see e.g. [1, 29], which can result in novel behaviour known as 'hidden' dynamics [14, 21].

Smoothing is mathematically desirable as it results in a differentiable system evolving in continuous time, governed by standard theorems of dynamical systems theory. From an applied perspective, however, this is highly idealised, and a switch may behave very differently if the system is discretised, or if the switch involves delay or hysteresis.

When modeling physical systems it is often important to factor in time-delays. If we return to section 2, we can set the discretization step $\varepsilon = 0$ but keep the delay σ (or τ) finite, to give a continuous time system with delay. Solutions of this will be trivial, as D_1 and D_0 shrink to the points $x = aT$ and $x = -bT$ which form a unique periodic orbit. The situation is not so trivial if there are two switches, perhaps with different delays. Some simulations in [18] reveal complex dynamics, but little is understood about how to characterise it at the time of writing.

Hysteresis (or spatial delay) is also of great importance in physical systems. This process has been well studied, first heuristically in [10, 32] and more rigorously in [2, 20]. The dynamics for one switch is trivial, bouncing between limits $x = \pm D$ for hysteresis of size D. For two switches this results in a billiard-like or 'chatterbox' problem that was well studied in [1], and this results in parameter-sensitive dynamics as highlighted in [20]; this is to our knowledge the only two-switch system where parameter dependence of the kind in section 5.2 has been proven analytically.

Perhaps more important from the viewpoint of computer simulation is what happens when we discretise a system. If we set the delay $\tau = 0$ in

section 2 but retain the discretization $\varepsilon > 0$, the resulting map obtained from (1) is a unit gradient 'map with a gap',

$$u_{n+1} = \begin{cases} f_1(u_n) = u_n - \phi & \text{if} \quad u_n > 0 \ , \\ f_0(u_n) = u_n + 1 & \text{if} \quad u_n < 0 \ , \end{cases} \tag{41}$$

a circle homeomorphism with well understood if already somewhat complex bifurcation structure, located at the accumulation of various bifurcation curves at $a_R = a_L = 1$ of the bifurcation diagram in Fig. 6.24 of [3]. In short this has intervals of periodic orbits if ϕ is rational, and dense quasiperiodic orbits if ϕ is irrational. Almost nothing is known in general about this situation if there are two switches.

Let us now consider what little is known if we combine any of these — smoothing, discretisation, hysteresis, delay — as we have done for discretization and delay in this paper.

6.2 Smoothing and hysteresis

Smoothing and hysteresis were in a sense combined in [4], in a unified model that exhibited either smooth or hysteretic behaviour in different limits. Although involving novel asymptotic balance of the competing limits, the dynamics itself is uninteresting, being consistent with the Filippov dynamics discussed in section 5.1. No such models have been studied for multiple switches, and it is not obvious whether the outcome would be as straightforward as for one switch, but it seems unlikely

6.3 Discretization and hysteresis

If we consider the system (5) and impose hysteresis of size D about $x = 0$, and discretise into time-steps ε, we have the map

$$x_{n+1} = \begin{cases} x_n + \epsilon a & \text{if} \quad x_n < D \ , \\ x_n - \epsilon b & \text{if} \quad x_n > -D \ . \end{cases} \tag{42}$$

If we re-scale by introducing $\phi = \frac{b}{a}$, $u = \frac{x}{\varepsilon a}$, $\delta = \frac{D}{\varepsilon a}$, then by steps similar to section 2 we obtain a map

$$\begin{aligned} &u_{n+k+j} = u_n - k\phi + j \ , \\ &\text{where} \qquad k = \left\lceil \frac{u_n + \delta}{\phi} \right\rceil \ , \quad j = \lceil k\phi + \delta - u_n \rceil \ . \end{aligned} \tag{43}$$

This is very similar to the delay map (10), and will have a similar family of topological types in the (δ, ϕ) plane leading to dynamics dependent on parameters as discussed in section 3.3. As in the discrete-delay process, this does not vanish as the step size ε is taken to zero.

For two switches we can expect similarly complex dynamics to that found with discretization and delay in section 4.2, but, as for that case, an explicit form for the map may not be possible.

6.4 Discretization and smoothing

It is common practice in many simulations of switching to first smooth out the switch, replacing any step function with a sigmoid function, and then discretise the equations for the purpose of numerical computation. Yet even this case can be less trivial than one may expect.

Take the usual starting point of (1), and replace $H(x)$ with some smooth sigmoid function $H_\sigma(x)$ that tends to $H(x)$ as $\sigma \to 0$ (we give some examples below). Then discretise in time-steps ε, to obtain the map

$$x_{n+1} = x_n + \varepsilon \left\{ a - (a+b) H_\sigma(x_n) \right\} \ . \tag{44}$$

This is simpler perhaps than the map (2), but similarly exhibits complex dynamics independent of $\varepsilon \to 0$, including chaos. The map has a fixed point x_* (corresponding to the sliding solution in the σ-neighbourhood of $x = 0$), given implicitly by

$$H_\sigma(x_*) = \frac{a}{a+b} \ . \tag{45}$$

This destabilises in a flip bifurcation where

$$\begin{aligned} & \frac{dx_{n+1}}{dx_n} = 1 - \varepsilon(a+b) H'_\sigma(x_n) = -1 \\ \Rightarrow \qquad & H'_\sigma(x_*) = \frac{2}{\varepsilon(a+b)} \ . \end{aligned} \tag{46}$$

For a typical sigmoid these two conditions have valid solutions, indicating that, for some σ/ε, a period doubling occurs, triggering a period doubling cascade.

For example, let $H_\sigma(x) = \frac{1}{2} + \frac{1}{2}\tanh(x/\sigma)$, then $H'_\sigma = \frac{2}{\sigma} H_\sigma (1 - H_\sigma)$ and the flip occurs at

$$\sigma = \frac{ab\varepsilon}{a+b} \ .$$

If we take the Hill function $H_\sigma(x) = (1+x)^{1/\sigma}/\left(1+(1+x)^{1/\sigma}\right)$, then $H'_\sigma = \frac{1}{\sigma}(1/H_\sigma - 1)^\sigma H_\sigma(1-H_\sigma)$ and the flip occurs at

$$\sigma = \left(\frac{b}{a}\right)^\sigma \frac{ab\varepsilon}{2(a+b)} \,.$$

These results assume a fixed time-step, and it may be of interest to study what happens with an adaptive step-size. Clearly the complex issue of regularising switches deserves further investigation in general.

7 Closing remarks

7.1 On sensitivity of nonsmooth dynamics

The importance of the variation shown throughout the analytical and numerical results above (from fig. 2 for the 1-switch system to fig. 14 for the 2-switch system), is that it constitutes an infinite sensitivity of the system to the parameters of the switching process. By this we mean that the behaviour of the system undergoes order 1 variations as the parameters τ (or $\tau_{1,2}$) change, independent of the small parameter ε, therefore persisting even when the delay and time-step are reduced as $\varepsilon \to 0$.

Our main result here has shown how this sensitivity to parameters results from considering the fine processes that accompany switching in dynamical systems. For one switch, this sensitivity reveals itself only in the transition between system modes, not in the large-scale dynamics. For two switches the sensitivity is evident both in the switching transitions and in the large-scale dynamics. In other words, we have shown that sensitivity already exists in the transition counts of the one-switch system, but it only becomes observable on the large-scale when there are two or more switches, upon which the times spend in each mode and the resulting sliding dynamics vary sensitively with parameters.

We derived explicitly how this happens for the specific situation of a discretised system with delays, and discussed what is known about the extension to other non-ideal models of switching.

One simplification we made in section 2 was to take only the leading order approximation of the vector field, resulting in a map with unit gradient. If we do not make this approximation and consider a varying vector field, the map (10) is qualitatively similar but with a non-unit gradient. The topological types and sensitive dynamics arise similarly, but an explicit map like (10) with both nonlinearity and delay in not known.

Instead, such a system can then be studied using the transition counts introduced for switching in section 5. This way of studying nonsmooth systems appears to hold great potential, being easily applied to any number of switches, and any kind of switching processes.

7.2 On transition counts versus time spent in modes

We saw above that the transition count matrix P_{hi} shows variability with the parameters of the switching process, for both the one and two-switch systems. Contrast this with the proportions of time μ (just μ for the one-switch system and μ_{ij} for two-switches), which only show variability in the presence of at least two switches. The theory of *nonsmooth* (or *piecewise-smooth* or *Filippov* or *variable structure*) systems, has typically focussed on these time proportions, rather than transition counts. The transition count reveals that the process of switching is inherently afflicted by variability, but because this does not affect the time proportions at a single switch, that variability has been hidden in much of the history of nonsmooth dynamics.

The two quantities are closely related, of course. That is, the time proportions μ spent in different modes, must be related to the transition counts P_{hi} between modes. Write the time proportions as a vector $\boldsymbol{\mu} = (\mu, 1-\mu)$ for one switch, or $\boldsymbol{\mu} = (\mu_{00}, \mu_{01}, \mu_{10}, \mu_{11})$ for two switches (with the normalization (36)), then

(i) the components of $\boldsymbol{\mu}$ sum to unity,

(ii) the rows of P_{hi} sum to unity, that is, $\sum_i P_{hi} = 1$,

(iii) $\boldsymbol{\mu}$ is the eigenvector of the transpose of P_{hi}, associated with unit eigenvalue and normalized according to (i), that is, $P^{\mathsf{T}}\boldsymbol{\mu} = 1\boldsymbol{\mu}$ or in components $\sum_h P_{hi}\mu_h = \mu_i$.

These properties of P_{hi} resemble those of the transition probability matrix of a Markov chain, and indeed, if the switching process is Markovian then the association is exact, and the spectral gaps studied in section 4 characterize the mixing time of the process. In our case, due to the delays, the process is not Markovian, however clearly P_{hi} plays a analogous role here, one whose theory we plan to extend in future work.

7.3 On types of switching

The obvious features that might be involved in the process of discontinuously switching modes across a threshold can be separated into certain types:

1. discrete but deterministic: hysteresis, delay, discrete time;

2. continuous deterministic: so-called Filippov systems, or regularisation by smoothing, or (not considered here but see e.g. [6, 9]) switching mediated by additional variables;

3. stochastic: e.g. additive noise, stochastic delay, fuzzy thresholds, stochastic decision making such as drift-diffusion.

We have covered class 1 here and shown they result in the most intricate dynamics around a switch. Class 2 has been studied at length and is much more regular in its behaviour. The two are apparently non-commensurate. Of class 3 little is known besides some preliminary simulations in [20, 18], and some results for special cases, e.g. border collision maps [13].

The problem studied here is an even more extreme simplification of the genetic regulation and investment games in [18], and the *pilots' dilemma* in [19]. These all begin with two 'controllers' or 'players' making simple decisions according to obvious logical rules. Although those rules govern the decisions made at any instant, as time passes, the logical outcome becomes lost in the problem's dynamical evolution, which becomes sensitive to the slightest intricacies of *how* the players' decisions interact, resulting in unpredictability.

These intricacies become a significant problem when we are dealing with networks of multiple decision makers. For example, is it even possible to define uniquely the sequencing of decisions made by controllers or players in a large distributed system? To do so requires a global clock on a network of switchable agents that defines simultaneity and ordering between the players, the precise timings or delays with which each agent acts, and how these may perturb the probability of their choices in response to each other. It might be obvious that differences in these might alter a large system's behaviour, but this work reveals that the dynamics of even a small system can be infinitely sensitive (since the small parameters can be taken arbitrarily small) to the simplest imperfections, even before more large-scale social factors like different agents' biases or beliefs might be taken into account. In future work we hope to look more at how the sensitivity derived here manifests in such decision problems.

Appendix

A The sampling problem

In fig. 5 we plotted the periodicity of the map (10) and its relation to the parameter ϕ. When the map has only a single jump this represents the winding number of the map, but how we sample ϕ in these plots affects their appearance. For instance, we might take ϕ values at regular intervals, or use Farey sequences to generate all rationals, or select random ϕ values. To highlight the issue and avoid mis-interpretation of the results, we show here plots for the same map obtained by sampling ϕ from the rationals in different ways.

In fig. 15 we plot the maximum period of the map (10) for all rational ϕ of the form p/q for $1 \leq q \leq Q$, taking $Q = 50$ and $Q = 100$ in the first two plots. The overall pattern is similar, but crucially the value of Q directly determines the maximum periods that are found, i.e. the height of the vertical axis (and trivially the latter plot also has more points).

More crucial, and perhaps less obvious, is that the patterns in these plots reflect not only the dynamics of the map, but are strongly influenced by the non-uniform distribution of taking all rational numbers up to a fixed denominator. To 'wash out' this influence we can instead sample values of ϕ in a more uniform manner. As an example, in the last plot of fig. 15 we randomly sample 1000 values of ϕ from the previous plot.

This shows that the overall maximum periodicity of these graphs is a reliable measure of the dynamics of the map *at those values*, but we must keep in mind that higher periods will be seen at ϕ values between these, becoming unbounded to indicate quasi-periodicity at irrational values between those. More importantly, the clear curve patterns in the top two graphs are indicative of the sampling of ϕ, not the variation of periodicities in the map itself, and hence do not appear in the last graph.

References

[1] J. C. Alexander and T. I. Seidman. Sliding modes in intersecting switching surfaces, I: Blending. *Houston J. Math*, 24(3):545–569, 1998.

[2] J. C. Alexander and T. I. Seidman. Sliding modes in intersecting switching surfaces, II: Hysteresis. *Houston J. Math*, 25(1):185–211, 1999.

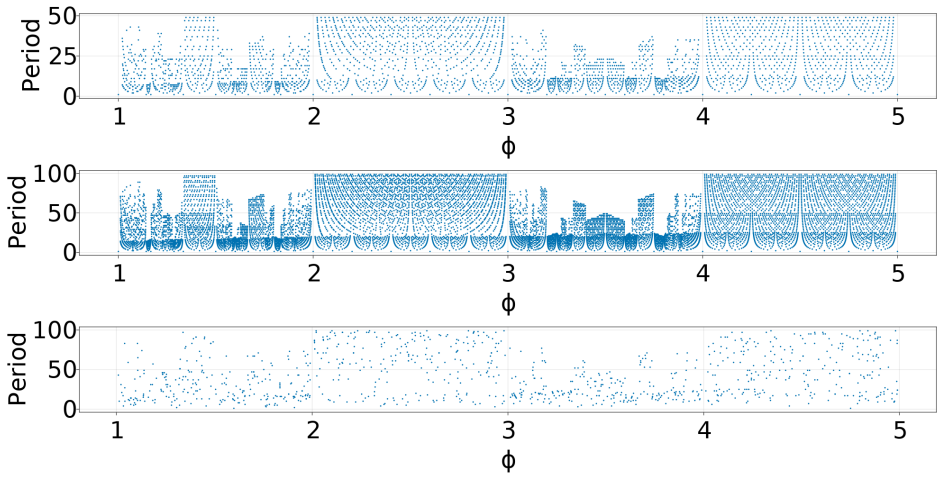

Figure 15: Maximum period of the map (10) with $\tau = 3$, for different values of ϕ. Top and middle: plotting all rational ϕ values with largest denominator 50 and 100, respectively. Bottom: ϕ is sampled from among the rationals with maximum denominator 100 (i.e. from middle plot) at 1000 randomly chosen points.

[3] V. Avrutin, L. Gardini, I. Sushko, and F. Tramantona. *Continuous and Discontinuous Piecewise-Smooth One-Dimensional Maps*, volume 95 of *Nonlinear Science Series A*. World Scientific, 2019.

[4] C. Bonet, T. M. Seara, E. Fossas, and M. R. Jeffrey. A unified approach to explain contrary effects of hysteresis and smoothing in nonsmooth systems. *Commun. Nonlin. Sci. Numer. Simul.*, 50:142–68, 2017.

[5] M. Boshernitzan and I. Kornfeld. Interval translation maps. *Ergod. Theory Dyn. Syst.*, 15:821–32, 1995.

[6] E. Bossolini, R. Edwards, P. Glendinning, M. R. Jeffrey, and S. Webber. Regularization by external variables. *Trends in Mathematics: Research Perspectives CRM Barcelona (Birkhauser)*, 8:19–24, 2017.

[7] R. Coutinho, B. Fernandez, R. Lima, and A. Meyroneinc. Discrete time piecewise affine models of genetic regulatory networks. *Journal of Mathematical Biology*, 52:524–70, 2006.

[8] L. Dieci and F. Difonzo. A comparison of Filippov sliding vector fields in codimension 2. *Journal of Computational and Applied Mathematics*, 262:161 – 179, 2014.

[9] R. Edwards, A. Machina, G. McGregor, and P. van den Driessche. A modelling framework for gene regulatory networks including transcription and translation. *Bull. Math. Biol.*, 77:953–983, 2015.

[10] A. F. Filippov. *Differential Equations with Discontinuous Righthand Sides*. Kluwer Academic Publ. Dortrecht, 1988 (original in Russian 1985).

[11] I. Flügge-Lotz. *Discontinuous Automatic Control*. Princeton University Press, 1953.

[12] R. Gesztelyi, J. Zsuga, A. Kemeny-Beke, B. Varga, B. Juhasz, and A. Tosaki. The Hill equation and the origin of quantitative pharmacology. *Arch. Hist. Exact Sci.*, 66:427–438, 2012.

[13] P. Glendinning. The border collision normal form with stochastic switching surface. *SIAM Journal on Applied Dynamical Systems*, 13(1):181–193, 2014.

[14] N. Guglielmi and E. Hairer. Classification of hidden dynamics in discontinuous dynamical systems. *SIAM J. Appl. Dynam. Sys.*, 14(3):1454–1477, 2015.

[15] A. V. Hill. The possible effects of the aggregation of the molecules of haemoglobin on its dissociation curves. *Proc. Physiol. Soc.*, 40:iv–vii, 1910.

[16] M. R. Jeffrey. Dynamics at a switching intersection: hierarchy, isonomy, and multiple-sliding. *SIAM J. Appl. Dynam. Sys.*, 13(3):1082–1105, 2014.

[17] M. R. Jeffrey. *Hidden Dynamics: The mathematics of switches, decisions, & other discontinuous behaviour*. Springer, 2019.

[18] M. R. Jeffrey. *Modeling with nonsmooth dynamics*. Frontiers in Applied Dynamical Systems. Springer Nature Switzerland, 2020.

[19] M. R. Jeffrey. Uncertainty in classical systems (with a local, nonstochastic, nonchaotic origin). *J. Phys. A*, 53(115701):1–15, 2020.

[20] M. R. Jeffrey, G. Kafanas, and D. J. W. Simpson. Jitter in dynamical systems with intersecting discontinuity surfaces. *IJBC*, 28(6):1–22, 2018.

[21] M. R. Jeffrey, T. I. Seidman, M. A. Teixeira, and V. I. Utkin. Into higher dimensions for nonsmooth dynamical systems. *Physica D*, 434(133222):1–13, 2022.

[22] J. Kilian and H. T. Siegelmann. The dynamic universality of sigmoidal neural networks. *Information and Computation*, 128(1):48–56, 1996.

[23] S. Kryzhevich, V. Avrutin, N. Begun, D. Rachinskii, and K. Tajbakhsh. Dynamics of systems with a discontinuous hysteresis operator and interval translation maps. *Axioms*, 10(2), 2021.

[24] J. Llibre, P. R. da Silva, and M. A. Teixeira. Sliding vector fields for non-smooth dynamical systems having intersecting switching manifolds. *Nonlinearity*, 28(2):493–507, 2015.

[25] G. Nikolsky. On automatic stability of a ship on a given course. *Proc Central Commun Lab (in Russian)*, 1:34–75, 1934.

[26] D. N. Novaes and M. R. Jeffrey. Regularization of hidden dynamics in piecewise smooth flows. *J. Differ. Equ.*, 259:4615–4633, 2015.

[27] J. Shi, J. Guldner, and V. I. Utkin. *Sliding mode control in electromechanical systems*. CRC Press, 1999.

[28] J. Sotomayor and M. A. Teixeira. Regularization of discontinuous vector fields. *Proceedings of the International Conference on Differential Equations, Lisboa*, pages 207–223, 1996.

[29] M. A. Teixeira and P. R. da Silva. Regularization and singular perturbation techniques for non-smooth systems. *Physica D*, 241(22):1948–55, 2012.

[30] V. I. Utkin. Variable structure systems with sliding modes. *IEEE Trans. Automat. Contr.*, 22:212–222, 1977.

[31] V. I. Utkin. *Sliding modes and their application in variable structure systems*, volume (Translated from the Russian). MiR, 1978.

[32] V. I. Utkin. *Sliding modes in control and optimization*. Springer-Verlag, 1992.

[33] R. A. Van Gorder. A theory of pattern formation for reaction–diffusion systems on temporal networks. *Proc. R. Soc. A.*, 477(2020075):1–28, 2021.

[34] V. Viktor, A. Panchuk, and I. Sushko. Border collision bifurcations of chaotic attractors in one-dimensional maps with multiple discontinuities. *Proc. R. Soc. A.*, 477(20210432):1–19, 2021.